

The DECam Minute Cadence Survey II: 49 Variables but No Planetary Transits of a White Dwarf

Kyra Dame¹, Claudia Belardi², Mukremin Kilic¹, Armin Rest³, A. Gianninas¹, Sara Barber⁴, Warren R. Brown⁵

¹*Homer L. Dodge Department of Physics & Astronomy, University of Oklahoma, 440 W. Brooks St, Norman, OK 73019, USA*

²*Department of Physics & Astronomy, University of Leicester, University Road, Leicester LE1 7RH, UK*

³*Department of Physics & Astronomy, The Johns Hopkins University, 3400 North Charles Street, Baltimore, MD 21218, USA*

⁴*House Committee on Science, Space, and Technology, 394 Ford House Office Building, Washington, DC 20515, USA*

⁵*Smithsonian Astrophysical Observatory, 60 Garden St, Cambridge, MA 02138, USA*

12 December 2021

ABSTRACT

We present minute cadence photometry of 31732 point sources observed in one 3 deg² DECam pointing centred at RA = 09:03:02 and Dec = -04:35:00 over eight consecutive half-nights. We use these data to search for eclipse-like events consistent with a planetary transit of a white dwarf and other sources of stellar variability within the field. We do not find any significant evidence for minute-long transits around our targets, hence we rule out planetary transits around ~ 370 white dwarfs that should be present in this field. Additionally, we identify 49 variables, including 40 new systems. These include 23 detached or contact stellar binaries, 1 eclipsing white dwarf + M dwarf binary, 16 δ Scuti, three RR Lyrae, and two ZZ Ceti pulsators. Results from the remaining two fields in our survey will allow us to place more stringent constraints on the frequency of planets orbiting white dwarfs in the habitable zone.

Key words: techniques: photometric, stars: variables: general, eclipses, white dwarfs

1 INTRODUCTION

Stellar variability on short timescales has been largely unexplored until recently, but is relevant in the era of transient surveys like the Zwicky Transient Facility (ZTF, Bellm & Kulkarni 2017), the Large Synoptic Survey Telescope (LSST, Ivezić et al. 2008), and in searches for optical counterparts to gravitational wave events detected by the Laser Interferometer Gravitational-Wave Observatory (*LIGO*). Exoplanet surveys like the Wide Angle Search for Planets (WASP, Pollacco et al. 2006) and the Hungarian-made Automated Telescope Network (HATNet, Bakos et al. 2004) have provided ~ 10 minute cadence observations of relatively bright stars, which can be used to search for transits around compact objects like white dwarfs (Faedi et al. 2011). On the fainter end, the Sloan Digital Sky Survey Stripe 82 (Bramich et al. 2008), the Panoramic Survey Telescope & Rapid Response System (Pan-STARRS) Medium Deep Fields (Tonry et al. 2012), and the Palomar Transient Factory (PTF, Rau et al. 2009) provided nightly observations of large areas of sky that were specifically designed to detect supernovae. Fulton et al. (2014) used the Pan-STARRS data on ~ 1700 photometrically selected candi-

dates to constrain the frequency of gas giant planets orbiting white dwarfs just outside the Roche limit (0.01 AU) to $< 0.5\%$, but their cadence and sensitivity were not high enough to constrain the frequency of Earth-size planets at the same orbital separation.

The Kepler/K2 mission has provided short-cadence, 1 min, data for hundreds of objects, but mainly for previously known pulsating stars. K2 long-cadence data led to the discovery of a disintegrating asteroid around the dusty white dwarf WD 1145+017 (Vanderburg et al. 2015; Gänsicke et al. 2016; Rappaport et al. 2016). Such planetesimals had never been found around white dwarfs previously due to a lack of extended duration high-cadence observations of a large number of white dwarfs. Van Sluijs & Van Eylen (2018) used long and short cadence K2 data from 1148 confirmed and high-probability white dwarfs to constrain the frequency of Earth-sized planets in the habitable zone around white dwarfs to $< 28\%$. For white dwarfs with masses between 0.4 and 0.9 M_{\odot} and $T_{\text{eff}} < 10000$ K, the continuously habitable zone (the region where a planet could sustain liquid water for > 3 Gyr) extends from ≈ 0.005 to 0.02 AU (Agol 2011).

The OmegaWhite Survey (Macfarlane et al. 2015, 2017;

Toma et al. 2016) is observing 400 deg² of the sky along the Galactic Plane with a median cadence of 2.7 min, with the goal of finding short period ($P_{orb} < 80$ min) variables, especially ultracompact binaries as these are predicted to be the strongest emitters of gravitational waves in the milli-Hertz frequency range (Amaro-Seoane et al. 2013; Roelofs et al. 2007). However, the 2 hour duration of their observations is not ideal for finding transits around white dwarfs as planets with such short periods would be tidally disrupted (Agol 2011).

The DECam Minute Cadence Survey (Belardi et al. 2016) was the first high cadence survey of its kind, observing 9 deg² of the sky at a cadence of ≈ 90 sec over 8 half-nights per field, specifically looking for transits around a large number of white dwarfs. Initial results from this survey focused on 111 high proper motion white dwarfs in their first 3 deg² field. While Belardi et al. (2016) did not find evidence of planetary mass companions to these high proper motion white dwarfs, they note that there should be hundreds of white dwarfs with low proper motion ($\mu < 20$ mas yr⁻¹) in the same field. Here we extract and analyse the photometry for all of the point sources in this field to search for transiting and variable objects, including the lower proper motion objects.

We discuss the details of our observations and reductions in Section 2. We discuss the results of our transit search in Section 3, present our selection process and list of variable objects in Section 4, and conclude in Section 5.

2 OBSERVATIONS AND DATA REDUCTION

2.1 DECam Observations

We used the Cerro Tololo Interamerican Observatory 4m telescope equipped with the Dark Energy Camera (DECam) over eight half-nights in Feb 2014. We obtained g -band exposures of a three square degree field, previously observed by the Canada-France-Hawaii Telescope Legacy Survey (CFHTLS, Cuillandre et al. 2012) with Megacam $ugriz$ photometry available. Our DECam field covers a small portion of the CFHTLS Wide 2 Field. Exposure times were chosen to obtain $S/N \geq 5$ photometry of targets brighter than $g = 24.5$ AB mag, giving an overall cadence of ≈ 90 s, including the 20 s read-out time of the camera. Further details of the observations can be found in Belardi et al. (2016).

2.2 Photometric Data Reduction

We downloaded the raw DECam data from the NOAO Archive and used the Photpipe pipeline, which was previously used in time-domain surveys like SuperMACHO, ESSENCE, and Pan-STARR1 (Rest et al. 2005; Garg et al. 2007; Miknaitis et al. 2007; Rest et al. 2014), to reduce these data. The pipeline performs single-epoch image calibration, including bias subtraction, cross-talk correction, flat-fielding, astrometric calibration, and geometrical distortion correction (using the SWarp software package, Bertin et al. 2002). It performs photometry using a modified version of DoPHOT (Schechter et al. 1993), and applies quality cuts to the resultant catalogue to remove stars less than 20

pixels from the edges of the CCDs, stars with a significantly brighter neighbour, and stars with photometric errors greater than 3σ (where σ is the mean photometric error of all objects in the corresponding 0.5 mag bin). Given our interest in variable objects, only relative photometry is needed, and we do not perform absolute photometric calibration.

2.3 Light Curve Creation

In order to remove the effects of short-term changes in the atmosphere (cloud coverage, haze, etc) and changes in airmass, we select ten bright, unsaturated, non-variable stars from each CCD to use as reference stars. For each CCD, we shift the light curves of our ten reference stars from that CCD to the same magnitude scale and apply a sigma-clipping algorithm to remove bad points affected by cosmic rays or CCD defects. We create a single reference light curve from the weighted means of the individual light curves. Sigma clipping is only used in the creation of our calibration light curve and is not applied to our sources in any subsequent steps. We then subtract this calibration light curve from every source identified in the corresponding CCD. The error introduced by our calibration procedure is two orders of magnitude smaller than the overall scatter in the light curves. Note that this process was run separately for each night.

Given that our reference stars are typically redder than white dwarfs, airmass-related effects are still visible in the light curves of many of our sources; these effects lead to significant peaks in the Fourier Transform, especially around 4 cycles per day (see Section 4.1). To remove this effect, we additionally fit a third-order polynomial to the calibrated source light curves.

2.4 Optical Spectroscopy

We obtained follow-up optical spectroscopy of two of the variable sources using the Blue Channel Spectrograph on the 6.5m MMT in October 2017. We operated the spectrograph with the 832 line mm⁻¹ grating in second order, providing wavelength coverage from 3600 Å to 4500 Å and a spectral resolution of 1.0 Å. We obtained all observations at the parallactic angle, with a comparison lamp exposure paired with every observation. We flux-calibrated using blue spectrophotometric standards (Massey et al. 1988).

We obtained follow-up optical spectroscopy of two additional variable sources using the Gemini Multi-Object Spectrograph on the 8m Gemini South telescope as part of the programme GS-2018A-Q-319. Observations were obtained using the B600 grating and a 1.0 arcsec slit, providing wavelength coverage from 3650 Å to 6750 Å and a spectral resolution of 3.6 Å. Targets were flux-calibrated using the spectrophotometric standard LTT7379.

3 TRANSITS

Planetary eclipses around white dwarfs should only last a few min, hence such events would only affect one or two data points per orbital period. Given the extremely short durations, traditional eclipse search algorithms like the box-least-squares periodogram are not a good way to identify

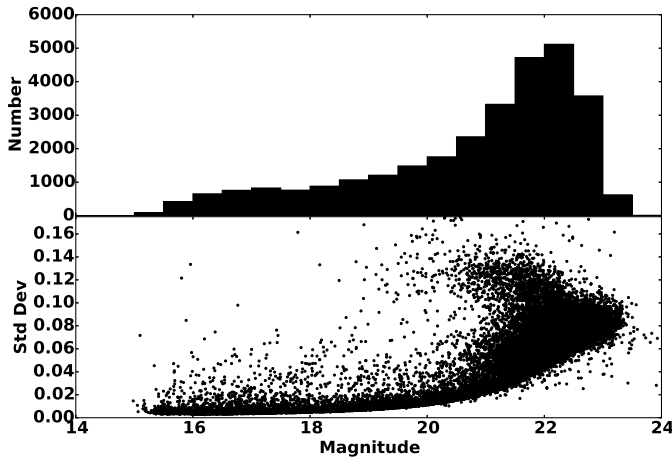


Figure 1. Magnitude distribution (top) and plot of standard deviation (bottom) of the light curve as a function of magnitude for the point sources included in our analysis. The hook feature seen in the standard deviation plot around $g=22$ mag is due to contamination from barely resolved sources.

white dwarf transits. Instead, a simple search for 5σ significant dips in flux is sufficient. However, identifying the source of these drop-outs, whether they are intrinsic to the source or not (due to instrumental or sky background problems), can be difficult. Using a 5σ threshold, Fulton et al. (2014) find 11,570 drop-outs (0.27%) out of 4.3 million data points in the Pan-STARRS Medium Deep Field data. However, further inspection of the images with the drop-out points show that none are compatible with eclipses by substellar companions to white dwarfs in those fields.

Figure 1 shows the magnitude distribution of the point sources in our first DECam field (top), as well as the standard deviation σ of the light curve of each source as a function of magnitude (bottom). This figure shows that our sample is incomplete beyond $g = 22.5$ mag. The hook feature seen around $g=22$ mag in the standard deviation plot is due to contamination from barely resolved sources in our sample. Even though the limiting magnitude of the individual DECam images is $g \approx 24$ mag, our data reduction pipeline only includes sources that are detected at a signal-to-noise ratio $S/N \geq 10$. This S/N ratio enables us to identify eclipses as shallow as 0.5 mag at 5σ confidence level, which is essential for finding Earth-size planets.

There are 31732 detections with point spread functions consistent with point sources in our DECam field. We have a total of 1024 images, which results in more than 30 million data points. We check each light curve for significant ($\geq 5\sigma$) dips and visually inspect the images with potential transits. We find 5244 potential transits, a significantly smaller fraction compared to the Fulton et al. (2014) study. However, our imaging pipeline already removes most sources near the edges and near bright, saturated stars. Visual inspection of these dips shows that the majority of these sources are either close to the edge of the chip, near bad pixels, or elongated, and are thus also not real. The point spread function is worse near the edges of the DECam field of view and it gets worse at high airmass (toward the end of the night). This explains

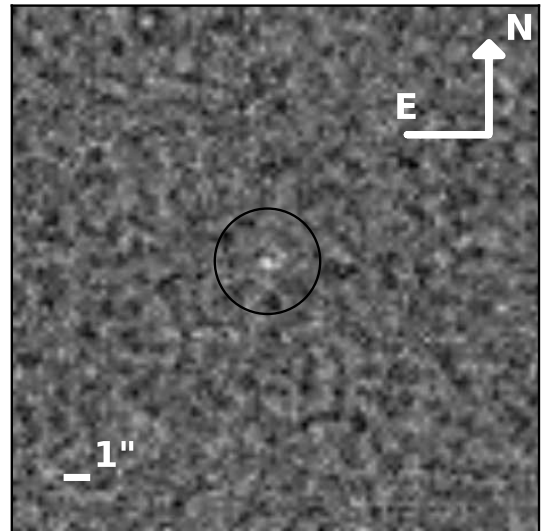
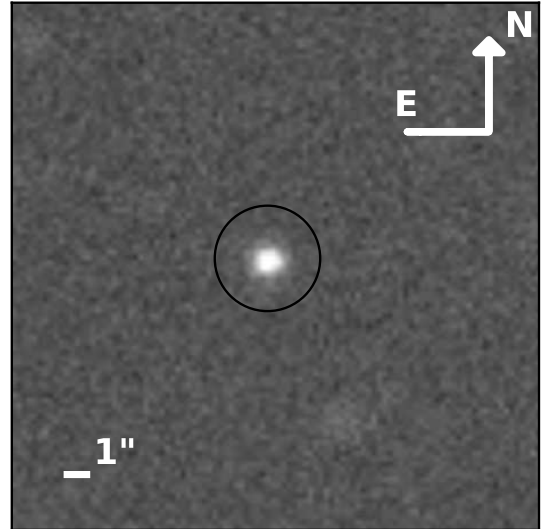


Figure 2. Image taken on UT 2014 Feb 05 at 05:21:18, corresponding to the drop-out candidate at RA = 09:07:10 and Dec = -04:29:44 (top) and the difference image (bottom). The target is circled.

many of the elongated images, which result in a lower flux measurement in our photometry.

Of our 5244 potential transits, we find eight that appear to be real, though interestingly, no source exhibits more than one genuine drop-out. However, even with a 5σ threshold and assuming gaussian errors, we still expect ≈ 18 such deviations in a sample of 30 million points simply due to random scatter. Hence, we expect to find about nine 5σ drop-outs. To determine whether these eight drop-outs are real, we vi-

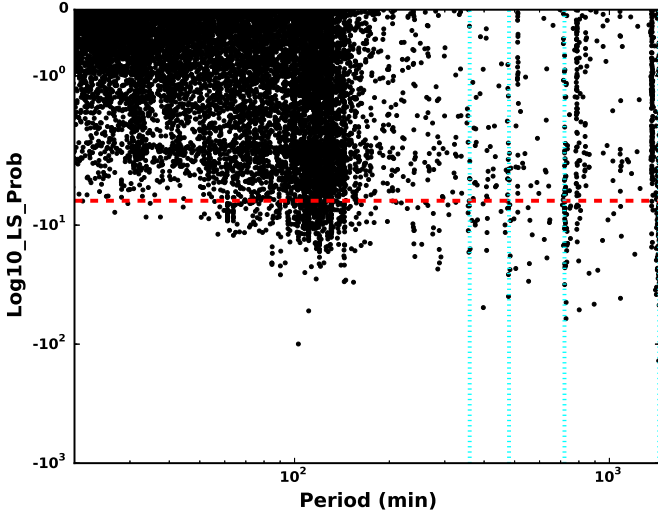


Figure 3. The false alarm probability ($\log_{10}(FAP)$) as a function of period for our sample. The red dashed line shows the theoretical 5σ confidence level; we select all objects below this line as our initial variable candidates. Cyan dotted lines mark periods of 6, 8, 12, and 24 hrs.

sually inspect difference images obtained with High Order Transform of PSF and Template Subtraction (HOTPANTS, Becker 2015). Figure 2 shows the image and difference image of an example drop-out candidate. We observe no corresponding dip in the difference images for our drop-out candidate, although it should be noted that for five of our eight drop-outs, the star is poorly subtracted. Therefore, while we do find eight dips consistent with a planetary transit of a white dwarf in our photometry, none of these dips appear significant to 3σ in the difference images so they are likely not real.

Of our 31732 targets, only 5011 are detected in *GAIA* Data Release 2 (Gaia Collaboration et al. 2018) with parallax over error ≥ 4 , and so *GAIA* is not useful for estimating the total number of white dwarfs in our field at these faint magnitudes. However, the Besançon Galaxy model (Robin et al. 2003) predicts 30381 stars with $13 \leq g \leq 24$ in our field, in good agreement with our 31732 detections. The model also predicts 374 white dwarfs within our field, giving a WD fraction of 1.23%. Belardi et al. (2016) calculated an expected detection rate of 0.7% due to the observing window from the ground for orbital periods less than 30 h. Therefore, based on these numbers, we would expect to find 2.6 planets in our sample if every white dwarf had an earth-mass planetary companion in its habitable zone.

4 VARIABILITY

4.1 Variable Candidate Selection

Using the VARTOOLS suite of software (Hartman & Bakos 2016), we run a Lomb-Scargle periodogram analysis on all the sources in the field. From this, we get the five most significant peaks in the periodogram and their corresponding false alarm probability (FAP). Figure 3 shows the distribu-

tion of $\log_{10}(FAP)$ values as a function of period for our sample. In theory, a star with $\log_{10}(FAP) = -6.2$ has a probability of being a variable object at the 5σ confidence level, with values more negative having higher probability of real variability. We use this limit to select our initial variable candidates. However, as discussed in Macfarlane et al. (2015), the 5σ confidence level can be more negative for real data than the theoretical limit due to systematic effects such as red noise, which introduces a larger spread in $\log_{10}(FAP)$ values at longer periods.

Of our 31732 sources, we find 889 variable candidates with at least one period with $\log_{10}(FAP) \leq -6.2$. However, as mentioned above, this is only a theoretical limit, and we expect the real 5σ confidence level to be more negative, especially at longer periods. Therefore, we use the Period04 package (Lenz & Breger 2014) to inspect each candidate. We compare the amplitudes of the observed peaks with the median amplitude, $\langle A \rangle$, of the Fourier Transform and look for significant peaks ($\geq 5\langle A \rangle$). Of our initial 889 candidates, 213 show no evidence of a significant peak upon inspection with Period04. For the remaining targets, we phase-fold the light curves to the period determined by Period04. Many of the resulting phase-folded light curves exhibit obvious problems due to attempts to fit outliers and minor zero-point magnitude differences across nights (due to our calibration method). Additionally, we see a significant number of false positives, occurring around 6, 8, 12, and 24 hours (see Fig. 3) due to our observing window from the ground. These problems result in poor phase coverage, and the light curves for these objects show no compelling evidence of variation at the periods and amplitudes determined.

However, we find 49 objects that do show genuine variability in their light curves. Table 1 presents the coordinates, periods, CFHT Legacy Survey *ugriz* photometry, and variable types for these sources. Note that for some, our method has difficulty finding an accurate period; most of these objects appear to have periods longer than our 4 hour nightly observing window, leading to poor phase coverage (see Section 4.3). However, their light curves do exhibit clear variability. For example, J0902–0510, J0903–0516, and J0905–0438 are eclipsing detached binary systems, but our phase coverage is not good enough to recover the binary period.

For the majority of our targets, we are able to determine the type of variable star from the colours, period, and general shape of the light curve. Figure 4 shows the colour-colour diagram for our variable targets, separated by type, along with all non-variable objects with $g < 20$ in the field, and the predicted colors¹ for pure hydrogen and pure helium white dwarfs (Holberg & Bergeron 2006; Kowalski & Saumon 2006; Tremblay et al. 2011; Bergeron et al. 2011). The CFHT Legacy Survey Wide 2 Field has low-extinction, $E(B-V) = 0.02$ mag. Hence, most pulsating stars (δ Scuti and RR Lyrae) cluster around relatively blue colors ($g-r \sim 0$), and are easy to identify, whereas detached and contact binaries involve stars with many different spectral types. Hence, these binaries appear everywhere along the stellar sequence.

Additionally, 45 of our variable sources were detected

¹ <http://www.astro.umontreal.ca/bergeron/CoolingModels/>

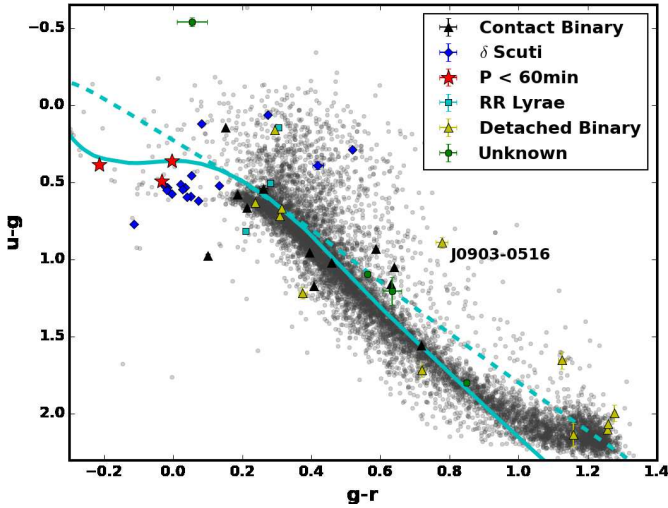


Figure 4. Colour-colour diagrams for our 49 variable objects and non-variable objects with $g < 20$ mag (grey points). Colors are taken from the CFHT Legacy Survey *ugriz* photometry (AB scale). Predicted colors for $\log g = 8.0$ white dwarfs with pure hydrogen atmospheres (solid line) and pure helium atmospheres (dashed line) are shown for reference. The white dwarf + M dwarf binary J0903–0516 is labelled.

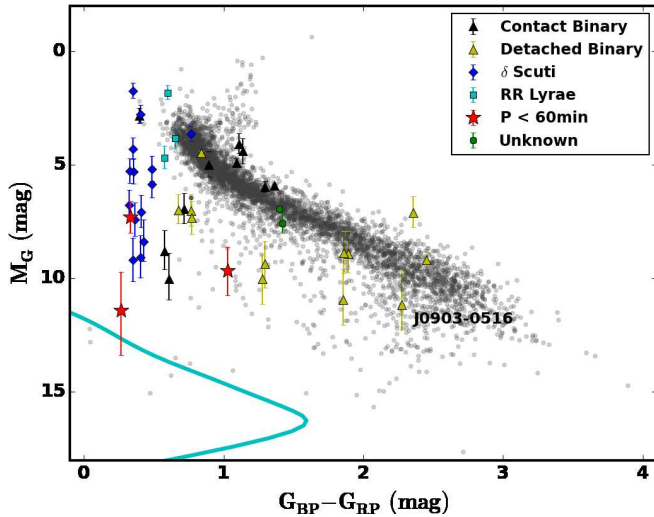


Figure 5. Colour-magnitude diagram for our 45 variable objects detected with *GAIA*. Symbols are the same as Figure 4. The 5001 non-variable sources from our survey with parallax over error ≥ 4 are shown as grey points. The cyan line shows the model sequence for a $0.6M_{\odot}$ H atmosphere white dwarf. The white dwarf + M dwarf binary J0903–0516 is labelled.

with *GAIA*. However, 11 have negative parallax values and only 10 have parallax over error ≥ 4 . We use the geometric distance estimates from Bailer-Jones et al. (2018), inferred from Bayesian analysis with a weak distance prior based on an exponentially decreasing space density such that the probability $P(r-L)$

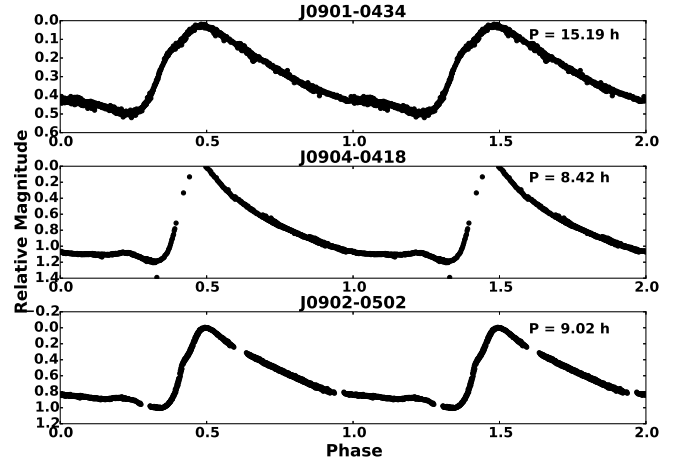


Figure 6. Phase-folded light curves for the three previously known RR Lyrae variables.

$$P(r|L) = \begin{cases} \frac{1}{2L^3} r^2 e^{-r/L}, & \text{if } r > 0 \\ 0, & \text{otherwise} \end{cases} \quad (1)$$

where r is the distance and $L > 0$ is a scale length.

In Figure 5, we show the colour-magnitude diagram for these 45 sources. We also include the 5001 non-variable sources (grey points) detected with *GAIA* with parallax over error ≥ 4 and the model sequence (cyan line) for a $0.6M_{\odot}$ H atmosphere white dwarf. The main sequence is clearly visible, and the positions of our variable sources show good agreement with our classifications.

In the following sections, we discuss our results for each variable type.

4.2 RR Lyrae

There are three previously known RR Lyrae in our field that were identified as part of the Catalina survey (Drake et al. 2013, 2014). Figure 6 shows the phase-folded light curves for these objects. They display ≥ 0.5 mag variations with periods ranging from 8 to 15 h. We recover, and independently confirm, the pulsation periods of these three objects in our DECAM data. Our phase-coverage for all three pulsators is excellent, demonstrating that we are able to identify variable stars at hour and \sim day long periods. We do not find any additional RR Lyrae in this field.

4.3 Contact and Detached Binaries

There are six previously known contact and detached binaries in our field that were identified by Drake et al. (2014). Figure 7 shows the phase-folded light curves for three of these objects. They display ≥ 0.15 mag variations with binary periods ranging from 6.1 to 28.6 h. Again, our phase coverage is excellent, and our observations cover $> 90\%$ of the binary orbit even for the longest period binary in this sample, J0905–0520 with $P = 28.6$ h.

Table 1. Coordinates, periods, *ugriz* photometry from the CFHT Legacy Survey, and determined variable type for out 49 variable candidates. Sources for previously known variables are provided.

Object	RA	Dec	Period (hr)	u	g	r	i	z	Type
<i>J0859</i> – 0439	08:59:37.250	–04:39:29.27	7.21	22.79	21.07	20.35	19.74	19.63	Detached
<i>J0900</i> – 0426	09:00:20.133	–04:26:27.36	46.15	22.43	21.21	20.84	20.21	20.30	Detached
<i>J0901</i> – 0350 ^c	09:01:03.319	–03:50:42.54	6.80	16.96	15.91	15.27	14.94	14.39	Contact
<i>J0901</i> – 0351	09:01:23.589	–03:51:06.45	21.82	19.66	18.94	18.63	18.51	18.52	Detached
<i>J0901</i> – 0352	09:01:29.915	–03:52:34.44	7.19	21.76	21.22	20.95	20.92	20.90	Contact
<i>J0901</i> – 0525	09:01:38.071	–05:25:05.08	96.00	19.16	18.53	18.29	18.21	18.48	Detached
<i>J0901</i> – 0457	09:01:56.909	–04:57:04.07	6.96	19.99	19.33	19.11	18.96	18.92	Contact
<i>J0902</i> – 0422	09:02:21.571	–04:22:42.30	60.00	22.78	20.79	19.51	18.65	18.41	Detached
<i>J0902</i> – 0439	09:02:45.974	–04:39:34.64	7.08	21.04	20.07	19.97	19.83	19.64	Contact
<i>J0902</i> – 0353 ^c	09:02:48.028	–03:53:03.22	7.60	18.10	16.93	16.52	16.51	15.91	Contact
<i>J0902</i> – 0510	09:02:57.061	–05:10:20.81	...	20.20	19.53	19.22	19.10	19.23	Detached
<i>J0903</i> – 0516	09:03:24.589	–05:16:53.25	...	22.72	21.83	21.05	19.70	19.10	Detached
<i>J0903</i> – 0429	09:03:42.089	–04:29:40.20	6.09	23.10	21.96	19.80	18.97	18.63	Detached
<i>J0903</i> – 0448	09:03:44.624	–04:48:32.97	14.04	21.91	19.81	18.55	17.40	16.96	Detached
<i>J0904</i> – 0415 ^c	09:04:07.252	–04:15:53.13	6.08	18.82	17.26	16.55	16.75	16.18	Contact
<i>J0904</i> – 0438	09:04:15.549	–04:38:03.73	6.22	18.80	17.64	17.01	17.07	16.62	Contact
<i>J0904</i> – 0429	09:04:31.582	–04:29:29.13	8.89	17.51	16.58	16.00	16.33	15.53	Contact
<i>J0904</i> – 0516 ^c	09:04:32.882	–05:16:57.97	10.17	15.97	15.82	15.67	15.64	15.65	Contact
<i>J0904</i> – 0404	09:04:37.052	–04:04:23.43	5.97	20.11	19.53	19.34	19.33	19.34	Contact
<i>J0904</i> – 0450	09:04:42.776	–04:50:55.14	7.29	20.57	19.55	19.09	19.11	19.11	Contact
<i>J0905</i> – 0520 ^c	09:05:09.954	–05:20:49.69	28.57	15.75	15.59	15.29	15.18	14.87	Detached
<i>J0905</i> – 0438	09:05:16.806	–04:38:18.66	...	21.82	19.75	18.50	17.49	16.83	Detached
<i>J0905</i> – 0511	09:05:49.293	–05:11:46.41	26.09	23.18	21.53	20.40	19.75	19.55	Detached
<i>J0905</i> – 0507 ^c	09:05:51.584	–05:07:08.31	8.51	18.74	17.78	17.39	17.34	17.25	Contact
Object	RA	Dec	Period (hr)	u	g	r	i	z	Type
<i>J0901</i> – 0434 ^b	09:01:41.200	–04:34:10.06	15.19	18.02	17.21	17.00	16.89	16.89	RR Lyrae
<i>J0902</i> – 0502 ^b	09:02:22.283	–05:02:01.24	9.02	17.98	17.48	17.20	17.36	17.49	RR Lyrae
<i>J0904</i> – 0418 ^b	09:04:57.676	–04:18:15.11	8.42	16.00	15.85	15.54	16.02	15.15	RR Lyrae
Object	RA	Dec	Period (min)	u	g	r	i	z	Type
<i>J0900</i> – 0444	09:00:22.458	–04:44:12.28	69.03	19.76	19.22	19.19	19.23	19.33	δ Scuti
<i>J0900</i> – 0358	09:00:33.589	–03:58:24.21	91.95	18.72	18.10	18.03	18.03	18.07	δ Scuti
<i>J0900</i> – 0456	09:00:49.936	–04:56:24.71	73.13	17.62	17.17	17.12	17.18	17.26	δ Scuti
<i>J0901</i> – 0437	09:01:53.875	–04:37:14.94	96.6	21.93	21.54	21.12	21.06	20.97	δ Scuti
<i>J0902</i> – 0351	09:02:33.540	–03:51:50.44	93.6	18.42	17.65	17.76	17.65	17.73	δ Scuti
<i>J0903</i> – 0519	09:03:16.452	–05:19:11.81	55.41	20.55	20.01	20.03	20.08	20.16	δ Scuti
<i>J0904</i> – 0506	09:04:11.330	–05:06:22.54	59.26	19.58	19.07	19.05	19.10	19.18	δ Scuti
<i>J0904</i> – 0442	09:04:29.256	–04:42:50.98	67.51	19.30	18.71	18.66	18.74	18.83	δ Scuti
<i>J0904</i> – 0423	09:04:50.248	–04:23:43.93	57.19	18.16	17.62	17.59	17.79	17.77	δ Scuti
<i>J0904</i> – 0515	09:04:50.834	–05:15:34.55	91.78	16.25	16.13	16.04	16.08	16.08	δ Scuti
<i>J0905</i> – 0437	09:05:28.246	–04:37:26.78	67.61	15.78	15.72	15.45	16.15	15.53	δ Scuti
<i>J0905</i> – 0433	09:05:35.177	–04:33:54.28	56.03	19.24	18.72	18.74	18.86	18.98	δ Scuti
<i>J0905</i> – 0430	09:05:40.849	–04:30:17.85	59.33	18.48	17.93	17.95	18.03	18.12	δ Scuti
<i>J0905</i> – 0458	09:05:45.608	–04:58:27.99	59.90	20.20	19.68	19.54	19.77	19.86	δ Scuti
<i>J0906</i> – 0407	09:06:21.666	–04:07:23.86	15.02	16.81	16.52	16.00	16.46	15.70	δ Scuti
<i>J0904</i> – 0532	09:04:15.727	–05:32:47.04	45.34	19.79	19.30	19.33	19.43	19.51	δ Scuti
			24.21						
Object	RA	Dec	Period (min)	u	g	r	i	z	Type
<i>J0859</i> – 0429	08:59:27.222	–04:29:16.34	7.76	20.93	20.54	20.76	20.91	21.06	ZZ Ceti
			5.30						
<i>J0900</i> – 0442 ^a	09:00:51.516	–04:42:49.18	14.46	20.97	20.60	20.61	20.11	19.67	ZZ Ceti
			12.62						
Object	RA	Dec	Period (min)	u	g	r	i	z	Type
<i>J0900</i> – 0352	09:00:53.225	–03:52:03.96	162.90	23.51	22.30	21.67	21.41	21.28	...
<i>J0902</i> – 0502	09:02:46.931	–05:02:45.10	...	16.98	15.89	15.33	15.16	14.71	...
<i>J0904</i> – 0516	09:04:02.124	–05:16:45.78	454.26	21.90	22.44	22.39	22.72	22.18	...
			83.38						...
<i>J0905</i> – 0511	09:05:08.181	–05:11:26.75	106.67	20.24	18.43	17.58	17.21	17.04	...

^a Belardi et al. (2016)^b Drake et al. (2013)^c Drake et al. (2014)

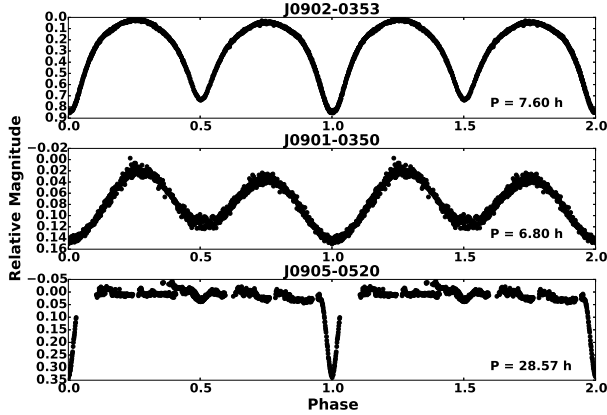


Figure 7. Phase-folded light curves for two previously identified contact binaries (top panels) and a detached binary (bottom panel) from Drake et al. (2014).

We identified an additional set of 18 new binary systems with our DECam data; 7 contact binaries and 11 detached binaries; these are shown in Figure 4 as black and yellow triangles respectively. Figure 8 shows example phase-folded light curves for four of our new contact and detached binary systems. The contact binaries have periods ranging from 6 to 9 hours, while the detached binaries have periods covering a much wider range, from 6 h to 4 days. However, for five of our 11 detached binaries, the periods are poorly constrained, and for another three, we could not determine a period at all. As mentioned above, this is likely due to poor phase coverage for longer orbital periods. For six of our 11 detached binaries, we observe only one or two transits over the entire eight half-nights (see Fig. 8); in comparison, our contact binaries have periods short enough to observe a transit every half-night, allowing for much better constraints on their orbital periods.

One of the new detached binaries involves an eclipsing compact object. Figure 9 shows our light curve for J0903–0516. We observe only a single transit, so we cannot determine a period. However, the short (≈ 30 min) duration and the sharp ingress and egress of the transit mark this object as a white dwarf + M dwarf binary. The observed light curve is essentially identical to the other eclipsing white dwarf + M dwarf binaries known (e.g., Parsons et al. 2017). About 22% of field white dwarfs have late-type stellar companions (Farihi et al. 2005), while 3.4% of these systems are eclipsing with $P < 2$ day orbits (Parsons et al. 2013). Hence, the frequency of eclipsing white dwarf + M dwarf binaries is likely around 0.75% for randomly oriented orbits. Given the predicted number of white dwarfs from the Besancon Galaxy model (see §4), we would expect to find up to 3 eclipsing white dwarf + M dwarfs in our dataset. Hence, the discovery of such a system in our survey is not surprising.

4.4 δ Scuti Type Pulsators

δ Scuti stars are the second most common type of variable stars in our survey. They typically have A-F spectral types and pulsation periods of 0.48-6 hrs (Chang et al. 2013). We find 15 objects with colours and periods consistent with δ Scuti type pulsators. These objects are shown as blue dia-

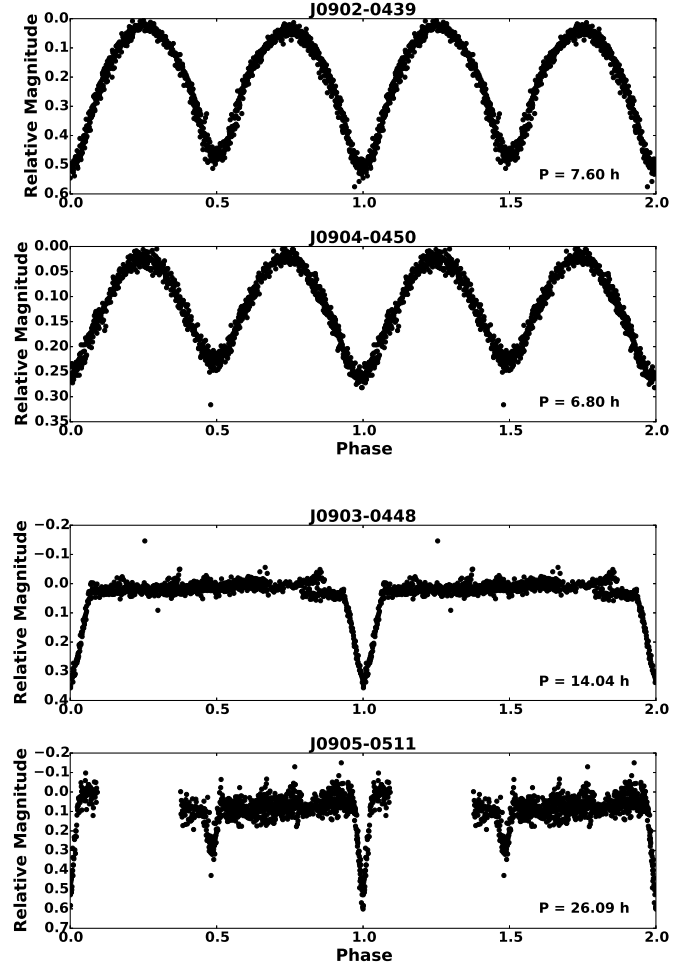


Figure 8. Representative phase-folded light curves for four of our new contact (top panels) and detached (bottom panels) binaries.

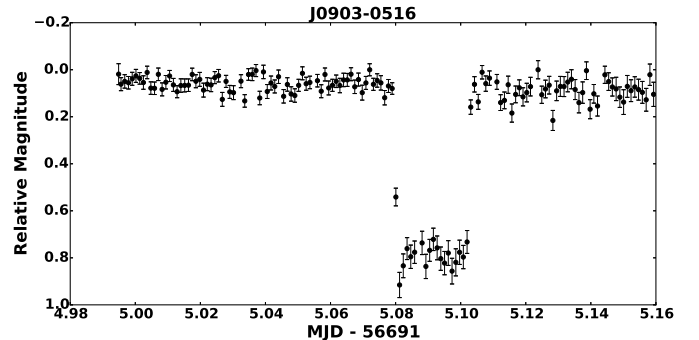


Figure 9. The single observed transit for the white dwarf + M dwarf binary J0903-0516.

monds in Figure 4. We show the phase-folded light curves for two of the newly identified δ Scuti type pulsators with periods near 1.6 h in Figure 10, and the light curves for a sample of the remaining from a single night in Figure 11.

All but one of these pulsators have periods ranging from 55 min to 97 min. However, there is a relatively red object, J0906-0407 with $g - r = 0.52$ mag, that shows variations

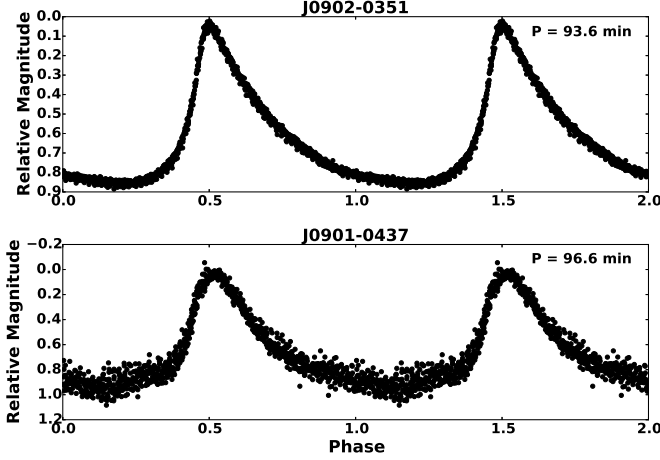


Figure 10. Phase-folded light curves for two of the newly identified δ Scuti type pulsators.

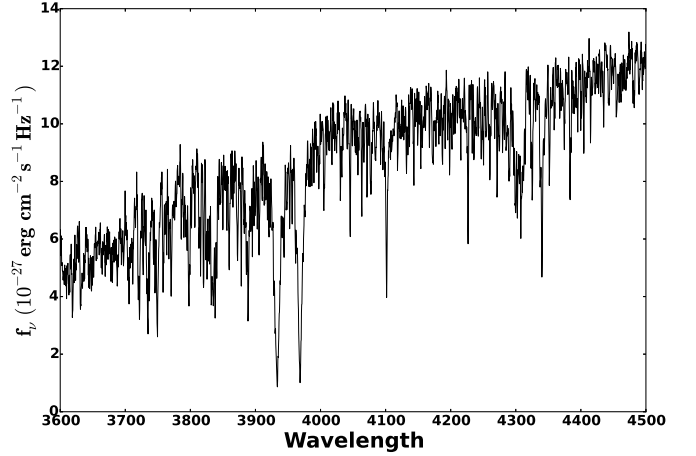


Figure 12. MMT spectrum of J0906-0407, a newly identified G-type δ Scuti pulsator.

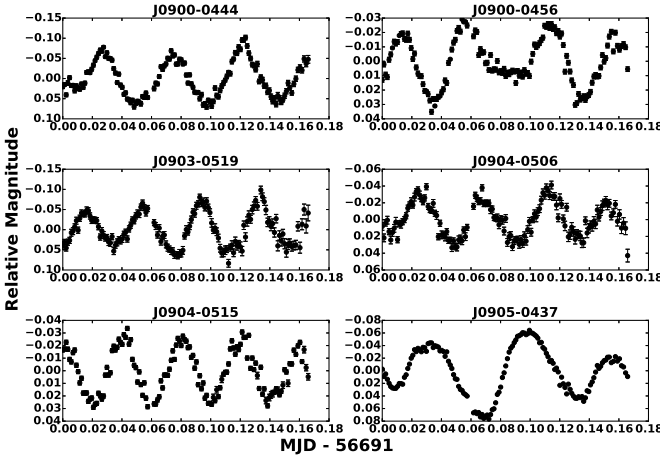


Figure 11. Light curves from a single night for 6 additional δ Scuti type pulsators in our DECam field.

with a dominant period of 15 min, which is near the period minimum of ≈ 18 min observed in the Kepler mission δ Scuti star sample (Uytterhoeven et al. 2011).

Given the relatively short period that could either indicate a pulsating ZZ Ceti white dwarf or a short period δ Scuti, we obtained follow-up spectroscopy of J0906-0407 to constrain its nature. Figure 12 shows its optical spectrum, which reveals strong Ca II H & K lines and the G-band absorption, as well as relatively weak H δ and H γ lines. Hence, J0906-0407 is clearly a G star. We compare the equivalent width measurements of these features to the spectral templates from Pickles (1998) and identify this object as a $\approx G0V$ star. Macfarlane et al. (2017) identify two δ Scuti pulsators with dominant periods of 9.0-9.6 min, including the G5 type star OW J075531.59-315058.2. Hence, J0906-0407 appears to be similar to other G-type δ Scuti stars with relatively short pulsation periods.

4.5 Short Period Pulsators

Among the 7 objects that cannot be readily identified by colour and period, we find three blue objects with short periods ($P < 60$ min). Their location in the $u - g$ versus $g - r$ color-color diagram (see Figure 4) is consistent with DA white dwarfs. Figure 13 shows the light curves and their Fourier transforms for two of these objects. The first is J0900-0442, the ZZ Ceti candidate previously discovered in Belardi et al. (2016) through its high proper motion. We detect two significant periods at 14.46 and 12.62 min, consistent with those found previously. Additionally, we find a second ZZ Ceti candidate in the field. J0859-0429 exhibits significant variations at 7.76 and 5.30 min, consistent with pulsation periods observed in other ZZ Ceti white dwarfs (Fontaine & Brassard 2008; Winget & Kepler 2008).

J0859-0429 has *ugriz* photometry that puts it right in the middle of the ZZ Ceti instability strip for white dwarfs (Gianninas et al. 2011) and J0900-0442 displays a proper motion of 27 mas yr^{-1} which puts it right in the middle of the white dwarf sequence in the reduced proper motion diagram (Belardi et al. 2016). As discussed in Belardi et al. (2016), the inability of the models to reproduce the SED of J0900-0442 may be due to an unseen companion. The remaining blue object that shows short period pulsations (at 24.21 and 45.34 min), J0904-0532, has colours consistent with a white dwarf, and its spectral energy distribution is well fit by a ≈ 8600 K object. These pulsation periods are longer than expected and the temperature is cooler than expected for average mass ZZ Ceti white dwarfs.

We obtained follow-up optical spectra of J0859-0429 and J0900-0442 from Gemini South, and J0904-0532 from MMT. The observed line profiles (black) and 1D model fits (red, Gianninas et al. 2011) are shown in Figure 14.

The normalised Balmer line profiles of J0859-0429 are best-fit by a pure H atmosphere model with $T_{\text{eff}} = 12940 \pm 690$ K and $\log g = 7.94 \pm 0.15$. These values are consistent with the instability strip for white dwarfs, confirming that J0859-0429 is a ZZ Ceti. Inclusion of H β in the fit yields $T_{\text{eff}} = 12400 \pm 410$ K and $\log g = 7.82 \pm 0.15$; the results are consistent within 1σ .

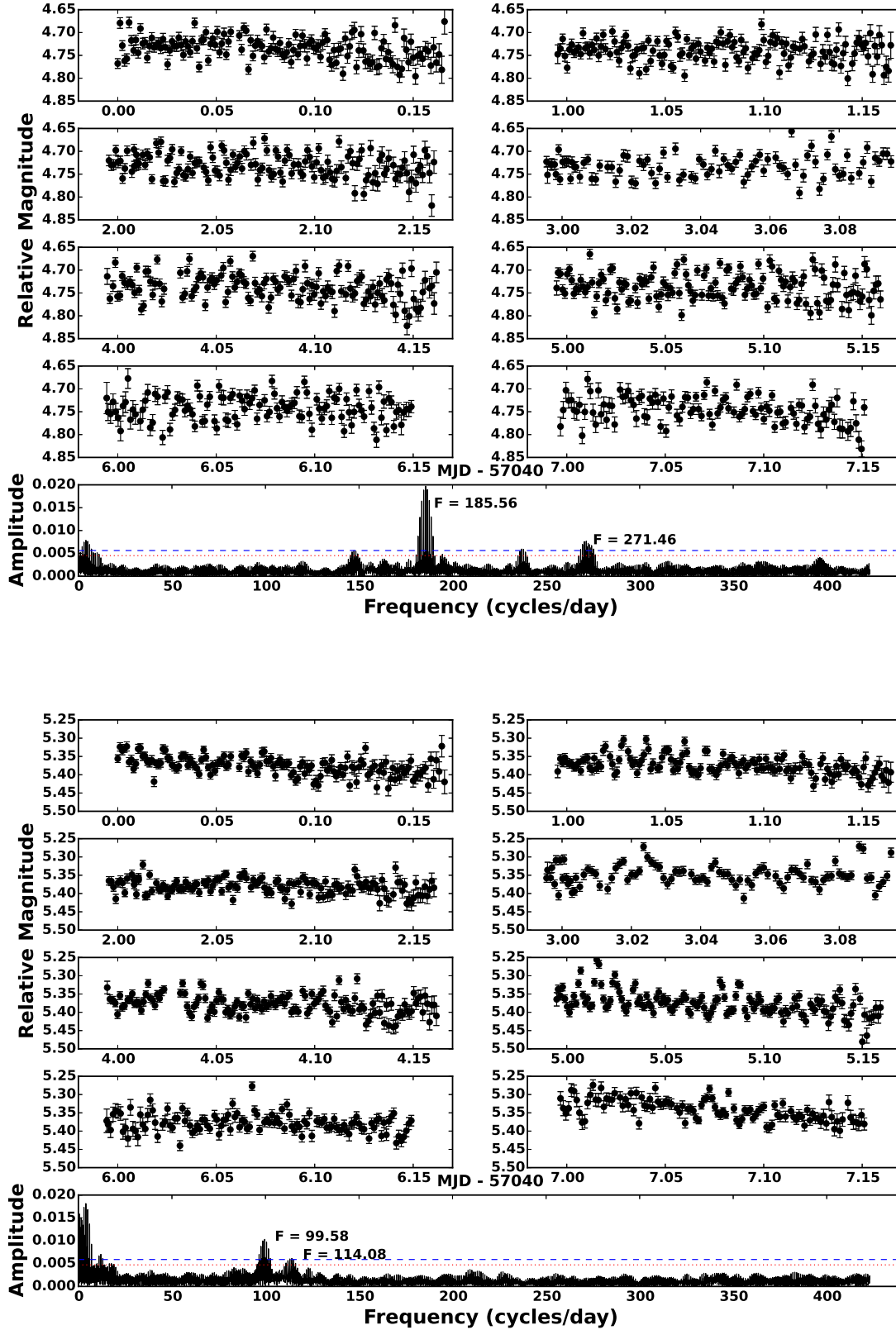


Figure 13. Light curves (top panels) and Fourier transforms (bottom panel) for J0859-0429 (top) and J0900-0442 (bottom). The red dotted line and blue dashed line in the Fourier transform show, respectively, the $4\langle A \rangle$ and $5\langle A \rangle$ detection limits, where $\langle A \rangle$ the median amplitude of the Fourier transform.

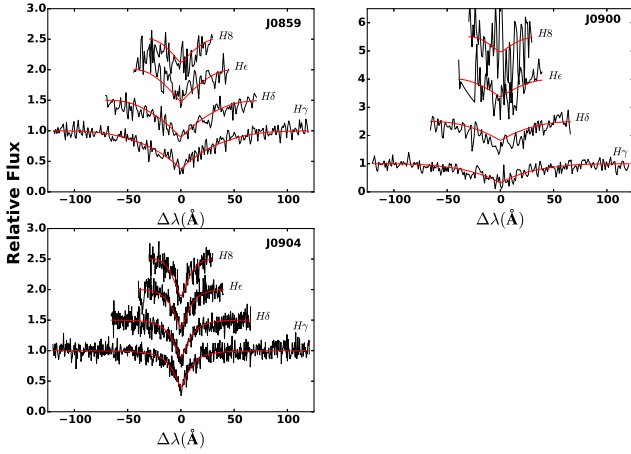


Figure 14. 1D model fits (red) to the observed Balmer line profiles (black) for J0859-0429 (top left), J0900-0442 (top right), and J0904-0532 (bottom left). For clarity, line profiles are vertically offset from each other.

The normalised Balmer line profiles of J0900-0442 are best-fit by a pure H atmosphere model with $T_{\text{eff}} \sim 12140$ K and $\log g \sim 6.85$. These values are broadly consistent with the instability strip; however, the errors are too large to unequivocally confirm that J0900-0442 is a ZZ Ceti. Since the SED of J0900-0442 shows contamination from a late type star, we do not include $H\beta$ in the fit.

The normalised Balmer line profiles of J0904-0532 are best-fit by a pure H atmosphere model with $T_{\text{eff}} = 8350 \pm 80$ K and $\log g = 5.46 \pm 0.16$. Fitting synthetic main-sequence star spectra with pure H atmosphere white dwarf models, Brown et al. (2017) demonstrate that these models systematically overestimate the surface gravity below 9000 K (Pelisoli et al. 2018). For example, the synthetic spectrum of a main-sequence star with $[\text{Fe}/\text{H}] = -1$, $T_{\text{eff}} = 8000$ K, and $\log g = 4.5$ is best-fit by a white dwarf model with $\log g \approx 5.1$. Hence, the model atmosphere fit is likely an overestimate of the actual surface gravity of this star. Additionally, its position in Figure 5 places it in the middle of the 15 δ Scuti type pulsators. Hence, J0904-0532 is certainly a δ Scuti type variable star.

4.6 Variables with Undetermined Types

There remains four objects for which we cannot determine the source of variability from colour and period alone. These objects are listed at the bottom of Table 1 and are marked by green circles in Figure 4. J0900-0352, J0902-0502, and J0905-0511 have colours consistent with main-sequence stars, but the light curves are simply too inconclusive to make a definitive identification. J0904-0516 has colours consistent with quasars; however, it exhibits variations with periods of 454.26 and 83.38 min, far shorter than the typical periods previously observed in quasars. Follow-up spectroscopy would be helpful in revealing the nature of these four objects, though two of them are relatively faint with $g > 22$ mag.

5 CONCLUSIONS

We present final results from the first field of the DECam minute-cadence survey. We construct light curves for the 31732 point source in the field, allowing us to search for potential planetary transits around otherwise difficult to identify low proper motion white dwarfs ($\mu < 20$ mas yr^{-1}). While we find no compelling evidence of such a transit around a white dwarf, we do identify 40 new variable objects: 18 binary systems (including a white dwarf + M dwarf binary), 16 δ Scuti type pulsators, and two ZZ Ceti white dwarfs. The remaining variable objects of undetermined type will require follow-up spectroscopic observations for reliable classification.

Analysis of the second and third fields is underway and will be presented in a future publication. We expect similar numbers of white dwarfs in the remaining two fields, allowing us to place stringent constraints on the frequency of Earth-sized planets in the habitable zone of white dwarfs. Additionally, surveys like SuperWASP, the Next-Generation Transit Survey, the Transiting Exoplanet Survey Satellite, and ZTF will obtain high-cadence observations for millions of stars. These observations will allow us to probe the variability of the night sky on timescales that remain largely unstudied, and open the possibility of observing previously unknown phenomena.

ACKNOWLEDGEMENTS

We thank the referee for their helpful suggestions. This work is in part supported by NASA under grant NNX14AF65G. Based on observations at Cerro Tololo Inter-American Observatory, National Optical Astronomy Observatory (NOAO Prop. ID:2014A-0073 and PI: M. Kilic), which is operated by the Association of Universities for Research in Astronomy (AURA) under a cooperative agreement with the National Science Foundation.

This project used data obtained with the Dark Energy Camera (DECam), which was constructed by the Dark Energy Survey (DES) collaboration. Funding for the DES Projects has been provided by the DOE and NSF (USA), MISE (Spain), STFC (UK), HEFCE (UK), NCSA (UIUC), KICP (U. Chicago), CCAPP (Ohio State), MIFPA (Texas A&M), CNPQ, FAPERJ, FINEP (Brazil), MINECO (Spain), DFG (Germany) and the collaborating institutions in the Dark Energy Survey, which are Argonne Lab, UC Santa Cruz, University of Cambridge, CIEMAT-Madrid, University of Chicago, University College London, DES-Brazil Consortium, University of Edinburgh, ETH Zurich, Fermilab, University of Illinois, ICE (IEEC-CSIC), IFAE Barcelona, Lawrence Berkeley Lab, LMU Munchen and the associated Excellence Cluster Universe, University of Michigan, NOAO, University of Nottingham, Ohio State University, University of Pennsylvania, University of Portsmouth, SLAC National Lab, Stanford University, University of Sussex, and Texas A&M University.

REFERENCES

Agol, E., 2011, ApJ, 731, L31

- Amaro-Seoane, P., Aoudia, S., Babak, S., et al. 2013, *GW Notes*, Vol. 6, p. 4-110, 6, 4
- Bailer-Jones, C. A. L., Rybizki, J., Fouesneau, M., Mantetlet, G., & Andrae, R. 2018, *AJ*, 156, 58
- Bakos, G., Noyes, R. W., Kovács, G., et al. 2004, *PASP*, 116, 266
- Becker, A. 2015, *Astrophysics Source Code Library*, ascl:1504.004
- Belardi, C., Kilic, M., Munn, J. A., et al. 2016, *MNRAS*, 462, 2506
- Bellm, E., & Kulkarni, S. 2017, *Nature Astronomy*, 1, 0071
- Bergeron, P., Wesemael, F., Dufour, P., et al. 2011, *ApJ*, 737, 28
- Bertin, E., Mellier, Y., Radovich, M., et al. 2002, *Astronomical Data Analysis Software and Systems XI*, 281, 228
- Bramich, D. M., Vidrih, S., Wyrzykowski, L., et al. 2008, *MNRAS*, 386, 887
- Brown, W. R., Kilic, M., & Gianninas, A. 2017, *ApJ*, 839, 23
- Chang, S.-W., Protopapas, P., Kim, D.-W., & Byun, Y.-I. 2013, *AJ*, 145, 132
- Cuillandre, J.-C. J., Withington, K., Hudelot, P., et al. 2012, *Proceedings of the SPIE*, 8448, 84480M
- Drake, A. J., Catelan, M., Djorgovski, S. G., et al. 2013, *ApJ*, 763, 32
- Drake, A. J., Graham, M. J., Djorgovski, S. G., et al. 2014, *ApJS*, 213, 9
- Faedi, F., West, R. G., Burleigh, M. R., Goad, M. R., & Hebb, L. 2011, *MNRAS*, 410, 899
- Farihi, J., Becklin, E. E., & Zuckerman, B. 2005, *ApJS*, 161, 394
- Fontaine, G., & Brassard, P. 2008, *PASP*, 120, 1043
- Fulton, B. J., Tonry, J. L., Flewelling, H., et al. 2014, *ApJ*, 796, 114
- Gaia Collaboration, Babusiaux, C., van Leeuwen, F., et al. 2018, *A&A*, 616, A10
- Gänsicke, B. T., Aungwerojwit, A., Marsh, T. R., et al. 2016, *ApJ*, 818, L7
- Garg, A., Stubbs, C. W., Challis, P., et al. 2007, *AJ*, 133, 403
- Gianninas, A., Bergeron, P., & Ruiz, M. T. 2011, *ApJ*, 743, 138
- Holberg, J. B., & Bergeron, P. 2006, *AJ*, 132, 1221
- Hartman, J. D., & Bakos, G. Á. 2016, *Astronomy and Computing*, 17, 1
- Hermes, J. J., Montgomery, M. H., Winget, D. E., et al. 2012, *ApJ*, 750, L28
- Ivezic, Z., Tyson, J. A., Abel, B., et al. 2008, *arXiv:0805.2366*
- Kaiser, N., Burgett, W., Chambers, K., et al. 2010, *Proceedings of the SPIE*, 7733, 77330E
- Kilic, M., Hermes, J. J., Gianninas, A., & Brown, W. R. 2015, *MNRAS*, 446, L26
- Kowalski, P. M., & Saumon, D. 2006, *ApJ*, 651, L137
- Lenz, P., & Breger, M. 2014, *Astrophysics Source Code Library*, ascl:1407.009
- Macfarlane, S. A., Toma, R., Ramsay, G., et al. 2015, *MNRAS*, 454, 507
- Macfarlane, S. A., Woudt, P. A., Groot, P. J., et al. 2017, *MNRAS*, 465, 434
- Massey, P., Strobel, K., Barnes, J. V., & Anderson, E. 1988, *ApJ*, 328, 315
- McNamara, D. H., Clementini, G., & Marconi, M. 2007, *AJ*, 133, 2752
- Miknaitis, G., Pignata, G., Rest, A., et al. 2007, *ApJ*, 666, 674
- Mukadam, A. S., Winget, D. E., von Hippel, T., et al. 2004, *ApJ*, 612, 1052
- Pelisolì, I., Kepler, S. O., & Koester, D. 2018, *MNRAS*, 470, 4473
- Parsons, S. G., Gänsicke, B. T., Marsh, T. R., et al. 2013, *MNRAS*, 429, 256
- Parsons, S. G., Gänsicke, B. T., Marsh, T. R., et al. 2017, *MNRAS*, 470, 4473
- Petersen, J. O., & Christensen-Dalsgaard, J. 1999, *A&A*, 352, 547
- Pickles, A. J. 1998, *PASP*, 110, 863
- Pollacco, D. L., Skillen, I., Collier Cameron, A., et al. 2006, *PASP*, 118, 1407
- Rappaport, S., Gary, B. L., Kaye, T., et al. 2016, *MNRAS*, 458, 3904
- Rau, A., Kulkarni, S. R., Law, N. M., et al. 2009, *PASP*, 121, 1334
- Rest, A., Stubbs, C., Becker, A. C., et al. 2005, *ApJ*, 634, 1103
- Rest, A., Scolnic, D., Foley, R. J., et al. 2014, *ApJ*, 795, 44
- Robin, A. C., Reylé, C., Derrière, S., & Picaud, S. 2003, *A&A*, 409, 523
- Roelofs, G. H. A., Nelemans, G., & Groot, P. J. 2007, *MNRAS*, 382, 685
- Schechter, P. L., Mateo, M., & Saha, A. 1993, *PASP*, 105, 1342
- Toma, R., Ramsay, G., Macfarlane, S., et al. 2016, *MNRAS*, 463, 1099
- Tonry, J. L., Stubbs, C. W., Kilic, M., et al. 2012, *ApJ*, 745, 42
- Tremblay, P.-E., Bergeron, P., & Gianninas, A. 2011, *ApJ*, 730, 128
- Uytterhoeven, K., Moya, A., Grigahcène, A., et al. 2011, *A&A*, 534, A125
- Vanderburg, A., Johnson, J. A., Rappaport, S., et al. 2015, *Nature*, 526, 546
- Van Sluijs, L., & Van Eylen, V. 2018, *MNRAS*, 474, 4603
- Winget, D. E., & Kepler, S. O. 2008, *ARA&A*, 46, 157